

# Orbital-resolved Soft X-Ray Spectroscopy in $\text{NaV}_2\text{O}_5$

G. P. Zhang

*Department of Physics and Astronomy, The University of Tennessee, Knoxville, TN 37996-1200*  
*Department of Physics, State University of New York, College at Buffalo, Buffalo, NY 14222\**

G. T. Woods<sup>1,2</sup> and Eric L. Shirley<sup>2</sup>

<sup>1</sup>*Department of Physics and Astronomy, The University of Tennessee, Knoxville, TN 37996-1200*

<sup>2</sup>*Optical Technology Division, National Institute of Standards and Technology,  
Gaithersburg, MD 20899-8441<sup>#</sup>*

T. A. Callcott, L. Lin and G. S. Chang

*Department of Physics and Astronomy, The University of Tennessee, Knoxville, TN 37996-1200*

B. C. Sales<sup>1</sup>, D. Mandrus<sup>1,2</sup> and J. He<sup>1,2</sup>

<sup>1</sup>*Solid State Division, Oak Ridge National Laboratory, TN 37831,*

<sup>2</sup>*Department of Physics and Astronomy, The University of Tennessee, Knoxville, TN 37996-1200*  
(October 28, 2018)

We demonstrate that angle-resolved soft x-ray spectroscopy can resolve absorption by inequivalent oxygen sites and by different orbitals belonging to the same site in  $\text{NaV}_2\text{O}_5$ . By rotating the polarization direction, we see a dramatic change in the absorption spectra at the oxygen  $K$  edge. Our theory identifies the detailed composition of the spectra and predicts a correct energy-ordering of the orbitals of three inequivalent oxygen atoms. Because different orbitals dominate absorption spectra at different energies and angles, one can excite at a specific site and “orbital”. In contrast, absorption at the vanadium  $L$  edge does not show large changes when varying the polarization direction. The reason for this is that different excitation channels (involving different initial states for the excited electron) overlap in energy and vary in compensating ways, obscuring each channel’s sensitive polarization dependence.

PACS: 78.70.Dm, 71.15.-m

## I. INTRODUCTION

Orbital degrees of freedom play a crucial role in many technologically interesting materials, such as superconductors, magnetic materials, and other strongly correlated compounds. For instance, the spin-orbit coupling effects determine whether the magnetic crystalline anisotropy in magnetic thin films favors magnetic moments normal or parallel to the surface of the sample. Such important effects motivate many investigations that probe orbitals in real materials. Soft x-ray spectroscopy (SXS)<sup>1–5</sup> has a unique capability to reveal spin and orbital information specific to one element. By employing x-ray magnetic circular dichroism, one can measure spin and orbital moments;<sup>6</sup> using x-ray magnetic linear dichroism, one can image antiferromagnetic domains at sub-micrometer scales.<sup>7</sup> Despite these tremendous achievements, imaging atomic orbitals has not often been done. The first attempt at the  $C K$  edge of graphite was done by Rosenberg *et al.*<sup>8</sup> A more elaborate study was performed a decade later with an intense synchrotron source.<sup>9</sup> On surfaces, the first investigation was made by Nilsson *et al.*<sup>10</sup> They used  $s$ -polarized soft x-rays to selectively excite  $\pi$  orbitals of CO adsorbed on Ni and used  $p$ -polarized light at off-normal angles to excite both  $\sigma$  and  $\pi$  orbitals, from which the orbital information could be extracted. However, obtaining such valuable orbital information in *bulk materials* is still a challenge for SXS.

In this work, we consider  $\text{NaV}_2\text{O}_5$ , a fascinating transition-metal compound that features three inequivalent oxygen sites:  $\text{O}_1$ ,  $\text{O}_2$  and  $\text{O}_3$  [cf Fig. 1(a)]. At 34 K, this material undergoes a spin-Peierls-like phase transition, which has attracted great interest.<sup>11–14</sup>  $\text{NaV}_2\text{O}_5$  is orthorhombic with symmetry of  $P_{mmm}$  and lattice constants  $a=11.316$  Å,  $b=3.611$  Å and  $c=4.797$  Å. It is a ladder structure compound along the  $b$  axis with  $\text{V-O}_1$ - $\text{V}$  bonds as its rungs extending along the  $a$  axis. The neighboring ladders along the  $b$  axis are connected by shifting a half-unit cell along the  $b$  axis. These ladders form quasi-two dimensional layers between which the sodium atoms are intercalated. One  $\text{O}_1$ , three oxygen  $\text{O}_2$  and one apical  $\text{O}_3$  atoms form a pyramid inside which one vanadium atom is situated. These three different oxygen atoms present a challenge to site-specific SXS, because one desires to obtain information, not only about different orbitals of atoms of different elements, but also about different orbitals on the same site.

Specifically, we report orbital-resolved x-ray absorption measurements, using the total electron yield method (TEY), on  $\text{NaV}_2\text{O}_5$  at the O  $K$  ( $1s$ ) and V  $L_3$  ( $2p_{3/2}$ ) edges. By changing the angle  $\theta$  between the electric field-polarization direction and certain crystal axes of  $\text{NaV}_2\text{O}_5$ , we can determine characteristic orbital energies, not only for orbitals on inequivalent O sites, but also for different orbitals on the same O site. With the aid of theoretical calculations, we are able to pinpoint the origin of the angular dependence of the O  $K$  edge absorption spectrum, distinguish different contributions thereto, and accurately determine the crucial energy ordering of the different orbitals from three inequivalent oxygen atoms. Combining different scans along different axes, we are able to project out spatial orientations of oxygen orbitals in real space. Thus, our study highlights an important capability of SXS that has not been explored in great detail.<sup>15</sup>

Our experiment reveals a surprising difference between the vanadium and oxygen edges. At the V  $L_3$  edge, the spectra show a very small dependence on  $\theta$ , but at the O  $K$  edge there is a large dependence. Our calculations are scalar-relativistic, so that we model the V  $L_{2,3}$  manifold without spin-orbit effects (including  $p_{1/2}-p_{3/2}$  splitting) taken into account. However, this description should still be able to address many aspects of a polarization dependence, which depends on states near the Fermi level. The theory shows that, subject to the dipole selection rule  $\Delta l = \pm 1$  and  $\Delta m = 0, \pm 1$ , transitions from  $s$  orbitals only have one initial state, i.e.,  $m = 0$ , while transitions from  $p$  orbitals have three initial states, i.e.,  $m = 0, \pm 1$ . Polarization dependences for absorption by electrons in each of the initial states compensate each other and ultimately lead to a very small polarization dependence. This explains the observed trend for the V  $L_3$  ( $2p_{3/2}$ ) edge.

The remainder of this article is arranged as follows. A brief review of our experimental measurements is described in Section II. In Section III, we present our theoretical scheme. The results and discussions are shown in Sec. IV. Finally, we conclude our paper in Section V. In a companion paper,<sup>16</sup> we analyze emission spectra and experimentally determine the occupied  $p$  density of states from each oxygen site. This paper is devoted entirely to the analysis of absorption spectra.

## II. EXPERIMENTAL MEASUREMENTS

Single crystals of  $\text{NaV}_2\text{O}_5$  were prepared at the Oak Ridge National Laboratory.<sup>16</sup> The crystals grow as rectangular platelets with the  $c$  axis normal to the plate surface, the  $a$  axis along the short side of the rectangle and  $b$  along the long side, as shown in Fig. 1(b). The samples were cleaved along the  $c$  axis. The experimental measurements were done at Beamline 8.0 of the Advanced Light Source at the Ernest Orlando Lawrence Berkeley National Laboratory.<sup>16</sup> The geometry of the measurements is indicated in Fig. 1(b). Horizontally polarized x-rays from an undulator and monochromator were incident on the sample. In the TEY detection mode, the x-ray absorption spectrum is measured by collecting the electrons that escape from the sample. Two samples were used in the experiment, and mounted at right angles to each other. Rotation of the sample holders scanned the polarization vector of the incident x-rays in the  $a$ - $c$  plane for one sample and in  $b$ - $c$  plane for the second sample.

$\text{NaV}_2\text{O}_5$  is an ideal system, in which to reveal a polarization dependence, because its structure is highly anisotropic. In Fig. 2, we show the normalized absorption spectra of a polarization scan from along the  $b$  axis to along the  $c$  axis, specifically from  $\theta = 7.5^\circ$  to  $\theta = 75^\circ$  with a step of  $7.5^\circ$ . For each angle, the normalization is done with respect to the total area between 514 eV and 536 eV because this energy region covers both the V-L and O-K edges.

We note that the TEY method has a finite sampling depth of about 100 Å. This suggests that our electron yield arises from a local spot of the sample. To illuminate the sample in the same place during measurement and to ensure data consistency, we adjusted the sample position after each change of its orientation angle. We found that data obtained using this technique are reproducible within 5 %.

We first consider the vanadium  $L_3$  edge around 518 eV [Fig. 2(a)]. When we scan the polarization from along the  $b$  axis to along the  $c$  axis, the spectra change very little. We observed a similar behavior when we scanned from along the  $a$  axis to along the  $c$  axis (not shown). However, for the oxygen  $K$  edge, we see a totally different picture [Fig. 2 (b)]. Increasing the angle  $\theta$  from  $7.5^\circ$  to  $75^\circ$  strongly changes the spectra. Three main peaks A, B and C, located at 530.6 eV, 532.1 eV and 532.8 eV, respectively, can be clearly identified. Peak A's intensity decreases sharply and eventually disappears as the polarization moves to along the  $c$  axis, which is normal to the sample surface. In the meantime, intensities of peaks B and C increase strongly and become the two main peaks on the spectra. To have a clear view of the intensity change, in Fig. 3 we plot the intensities versus angle  $\theta$  for those three peaks. Their variations can be nicely fitted to a  $\cos 2\theta$  dependence, which is the simplest possible variation (see the solid lines in Fig. 3).

### III. THEORETICAL FRAMEWORK

Our theoretical calculation to simulate the experiment is based on pseudopotential,<sup>17</sup> local-density-approximation (LDA) calculations.<sup>18</sup> Electron states are found by solving the self-consistent Kohn-Sham (KS) equations,

$$\hat{H}\Psi_{n\mathbf{k}}(\mathbf{r}) = \left\{-\frac{\hbar^2}{2m}\nabla^2 + \hat{V}_{\text{eff}}\right\}\Psi_{n\mathbf{k}}(\mathbf{r}) = E_{n\mathbf{k}}\Psi_{n\mathbf{k}}(\mathbf{r}) \quad (1)$$

Here  $\Psi_{n\mathbf{k}}$  is the Bloch state for an electron in band  $n$  at crystal wave-vector  $\mathbf{k}$ . The effective potential is given by

$$\hat{V}_{\text{eff}} = V_{\text{ion}} + V_{\text{H}}(\mathbf{r}) + V_{\text{xc}}(\mathbf{r}). \quad (2)$$

The three terms account for the pseudopotential interaction of electrons with ion cores  $V_{\text{ion}}$ , the Hartree potential  $V_{\text{H}}(\mathbf{r})$  that is obtained from the electron charge density, given by

$$n(\mathbf{r}) = \sum_{n\mathbf{k}}^{\text{occ'd.}} |\Psi_{n\mathbf{k}}(\mathbf{r})|^2 \quad (3)$$

and exchange and correlation effects  $V_{\text{xc}}$ . We use the Ceperley-Alder form<sup>19</sup> for the exchange term  $V_{\text{xc}} = \delta E_{\text{xc}}[n]/\delta n(\mathbf{r})$ . The ionic potential  $V_{\text{ion}}$  is a norm-conserving pseudopotential computed within the Hartree-Fock approximation, and with core-valence correlation effects included using the core-polarization-potential method.<sup>20</sup> As basis sets, we use plane waves or optimized basis functions.<sup>21</sup>

To compute an x-ray absorption spectrum, we use the expression,<sup>1,5</sup>

$$S(\omega) \propto 2\pi \sum_f |\langle f|\mathbf{p} \cdot \mathbf{A}|i\rangle|^2 \delta(\omega + E_i - E_f) \quad (4)$$

where  $\mathbf{p} \cdot \mathbf{A}$  is the electron-photon interaction approximated by a dipole operator;  $|i\rangle$  is the initial core state with energy  $E_i$ ,  $|f\rangle$  is the final state with energy  $E_f$ , and  $\omega$  is the incident photon energy. In our present analysis, which mainly deals with determining the symmetries of orbitals, we neglect electron-core hole interactions in the final state.

### IV. RESULTS AND DISCUSSIONS

#### A. Oxygen $K$ (1s) edge absorption spectrum

In the experiment, we always rotated our polarization direction from along the  $b$  axis to along the  $c$  axis in the way already described. Theoretically, we did calculations in the same way. In Fig. 4(a), we show theoretical x-ray absorption spectra at the O  $K$  edge, where three peaks, A, B and C, are also clearly observed with different intensities as a function of polarization. The spectra were calculated with  $12 \times 12 \times 12$  k-point meshes. The results are found well-converged. The angular dependence of these peaks is in good agreement with the experimental observations: Peak A decreases as the polarization moves away from along the  $b$  axis, whereas both peaks B and C increase. The change also follows a cosine function of  $\theta$ , consistent with the experimental observation. Note that the experimental measurements cannot directly determine which oxygen orbitals contribute to these main peaks, whereas calculations should provide important insight into this.

Figures 4(b-d) show the respective contributions from three inequivalent oxygen sites. To simplify our notation, we let  $O_m(P_n)$  denote the  $n$ th orbital of oxygen  $O_m$  that participates the absorption process. That is, the local, partial density of states for such an orbital can play a significant role in absorption as a function of excitation energy, and this role can be strongest at some ‘‘characteristic’’ energy. We first consider peaks B and C. By comparing Fig. 4(a) with Figs. 4(b), 4(c) and 4(d), we infer that peaks B and C in Fig. 4(a) and Fig. 2(b) originate from  $O_1(P_3)$ ,  $O_2(P_4)$ ,  $O_2(P_5)$ , and  $O_3(P_5)$  orbitals, whose characteristic orbital energies (expressed relative to the O 1s level) are 533.0 eV, 533.1 eV, 533.7 eV and 533.1 eV, respectively.

When considering peak A in Figs. 4(a) and 2(b), we notice that all three inequivalent atoms contribute but are favored in different ranges of energy. Figure 4(b) illustrates the main contributions from  $O_1$ . It is important to note that only  $O_1(P_1)$  appears at 530.2 eV, which helps us to resolve different orbital contributions (see next paragraph). The peak intensity decreases as the polarization direction deviates from the  $b$  axis, in a similar way as peak A in Fig. 2(b) or Fig. 4(a).  $O_1(P_1)$  is immediately followed by  $O_3(P_1)$  at 530.6 eV with an energy difference between them of about 0.4 eV, [cf. Fig. 4 (d)]. The  $O_3(P_1)$  intensity changes in a similar manner as does that for  $O_1(P_1)$ . After

the  $O_3(P_1)$  orbital, the  $O_2(P_3)$  orbital gradually appears around 531 eV to 532 eV [cf. Fig. 4(c)]. Because of their unique positions,  $O_2$  orbitals are distorted, and not along one particular axis. Thus, the angular dependence of their contribution to absorption is weaker than for orbitals on  $O_1$  and  $O_3$ .

These results show that the measured peak A has contributions from the  $O_1(P_1)$ ,  $O_3(P_1)$ , and part of  $O_2(P_3)$  orbitals. This could prove crucial for our tentative explanation of emission spectra that is given subsequently in Ref. 16. In particular, because our theory shows that these three orbitals have different energies, it is possible to excite different orbitals at different energies and to *resolve* them experimentally. This is exactly what we did. Because the energy increases in the order of  $O_1$ ,  $O_3$  and  $O_2$ , we can selectively excite these atoms. When we excite at the  $O_1(P_1)$  orbital edge, we only see one peak in the emission spectrum, because  $O_2$  and  $O_3$  atoms are not excited, though in the normal fluorescence spectrum, we expect to see two main peaks. Therefore, with theoretical guidance, we demonstrate that we are able to *resolve* these *different* orbitals associated not only with different sites such as  $O_1(P_1)$ ,  $O_3(P_1)$ ,  $O_2(P_3)$  but also with the *same* site such as  $O_1(P_1)$  and  $O_1(P_3)$ .

By scanning polarization from along the a axis to along the b axis and from along the a axis to along the c axis, we can project out orbital orientations in real space. Putting together all the results, we can show some of the orbitals in the real space in Fig. 5. One sees that there are two kinds of  $O_3$  orbitals: one is along the a axis, the other is along the c axis, and one  $O_1$  orbital along the b axis, two  $O_2$  orbitals along the b and a axes. Note that, unlike charge-density plots for orbitals, the orbitals presented here are experimentally accessible. Thus, we demonstrate that the soft x-ray spectroscopy has the capability of resolving orbitals from the same site.

## B. Vanadium $L_3$ ( $2p_{3/2}$ ) edge

The x-ray absorption spectrum at the V  $L_3$  edge is rather unique and shows a very weak angular dependence. At room temperature, there is only one inequivalent vanadium atom. In our scalar-relativistic calculations, excitation of V 2p electrons can involve three electron initial states:  $m = 0, \pm 1$ . Our absorption spectrum intrinsically involves a sum over excitations with the indicated initial states, and the experimentally observed spectrum is an analogous sum at the V  $L_3$  edge. We first show the results of the first channel in Fig. 6(a). We note that with the incident polarization turning away from the b axis, the whole spectrum clearly changes. If this were the dominant excitation channel, then one would see a strong angular dependence in experiment. However, our experiment showed otherwise, which implies that we should take into account the other channels. In Fig. 6(b), we plot the change because of the  $l = 1, m = \pm 1$  channel. Without spin-orbit coupling, the spectra for both  $l = 1, m = +1$  and  $l = 1, m = -1$  channels are same. Two prominent features are: (1) the mean peak strongly overlaps the spectra of the  $l = 1, m = 0$  channel; (2) the portion showing strong angular dependence is on the right-hand side, which is opposite to that in Fig. 6(a). Because of this compensating effect, the total absorption spectrum does not show a strong angular dependence as one can see in Fig. 6(c). This explains our experimental observations.

Now comparing this with the oxygen  $K$ -edge spectra where only one excitation channel,  $l = 0$  and  $m = 0$ , participates in the process, we clearly see that appropriate summation over the multiple excitation channels (i.e., corresponding to different electron initial states) obscures the polarization dependence, which ultimately leads to the big difference between the role of polarization at the V  $L_3$  edge vs the O  $K$  edge. This finding demonstrates the importance of understanding selection rules in x-ray spectroscopy, and it might help one optimize the polarization direction to reveal the maximal information from x-ray spectroscopy measurements in the future. In particular, it would be interesting to ask whether the present polarization effects for the various components of the V  $L_3$  spectrum could be resolved by circular dichroism. However, the difficulty is that even with the 2p core spin-orbit coupling, in the absence of spin-polarization of the V-d bands,  $\Delta m = \pm 1$  transitions should also be the same.

## V. CONCLUSIONS

In conclusion, we measured angular dependence of x-ray absorption spectra at the vanadium  $L_3$  edge and oxygen  $K$  edge. Rotating the polarization from along the b axis to along the c axis, the spectra at these two edges behave quite differently. There is very little change at the V  $L_3$  edge, while a dramatic change is observed at the O  $K$  edge. Such a large change enables us to selectively excite different orbitals belonging to the same site. Thus, we are able to *resolve orbitals* for the *same* element using soft x-ray spectroscopy. Our theoretical calculation provides the detailed information to understand the experimental spectra. It clarifies how the predominant first peak at the oxygen  $K$  edge is from three different orbitals of three different oxygen sites ( $O_1$ ,  $O_2$  and  $O_3$ ) and determines the crucial energy ordering of the orbitals on these sites. This also helps explain the emission spectra. Our calculations also show how a compensating effect can arise in the polarization dependence of various excitation channels for the V  $L_3$  edge, so

that the total absorption spectrum at the edges exhibits a small polarization dependence. After we submitted this paper, we noticed three recent papers<sup>22</sup> that intensively debated whether the anomalous scattering factors in the x-ray diffraction technique could be used to probe the charge ordering in  $\text{NaV}_2\text{O}_5$ . Our study shows that if excited at the  $V L_3$  edge, the orbital or structural effects are small. Thus, one might explain the anomalous scattering as resulting from the charge ordering, provided that the scattering intensity of the charge ordering is larger than that of the orbital ordering.

### Acknowledgment

This research is supported by NSF DMR-9801804 and NSF DMR-0072998. Oak Ridge National Laboratory is managed by UT-Battelle, LLC, for the U.S. Department of Energy under Contract No. DE-AC05-00OR22725. Measurements were carried out at the Advanced Light Source at the Ernest Orlando Lawrence Berkeley National Laboratory, supported U.S. Department of Energy Contract DE-A003-76SF00098. We would like to acknowledge Christen Halloy and the staff at the Joint Institute of Computational Sciences (JICS) at the University of Tennessee at Knoxville, where part of calculation has been done.

\*Mailing address

#Present address

- 
- <sup>1</sup> T. A. Callcott, in *Vacuum Ultraviolet Spectroscopy II*, ed. by J. A. Samson and D. L. Ederer, Experimental Methods in the Physical Sciences, Vol. 32 (Academic Press, New York, 1998), p. 279.
- <sup>2</sup> J. J. Jia, T. A. Callcott, E. L. Shirley, J. A. Carlisle, L. J. Terminello, A. Asfaw, D. L. Ederer, F. J. Himpsel, and R. C. C. Perera, Phys. Rev. Lett. **76**, 4054 (1996).
- <sup>3</sup> J. A. Carlisle, E. L. Shirley, E. A. Hudson, L. J. Terminello, T. A. Callcott, J. J. Jia, D. L. Ederer, R. C. C. Perera, and F. J. Himpsel, Phys. Rev. Lett. **74**, 1234 (1995).
- <sup>4</sup> T. A. Callcott and E. T. Arakawa, Phys. Rev. B **18**, 6622 (1978).
- <sup>5</sup> A. Kotani and S. Shin, Rev. Mod. Phys. **73**, 203 (2001).
- <sup>6</sup> P. Carra, B. T. Thole, M. Altarelli and X. Wang, Phys. Rev. Lett. **70**, 694 (1990).
- <sup>7</sup> J. Stöhr, A. Scholl, T. J. Regan, S. Anders, J. Lüning, M. R. Scheinfein, H. A. Padmore, and R. L. White, Phys. Rev. Lett. **83**, 1862 (1999); A. Scholl, *et al.* Science **287**, 1014 (2000).
- <sup>8</sup> R. A. Rosenberg, P. J. Love and V. Rehn, Phys. Rev. B **33**, 4034 (1986).
- <sup>9</sup> P. Skytt, P. Glans, D. C. Mancini, J.-H. Guo, N. Wassdahl, J. Nordgren, and Y. Ma, Phys. Rev. B **50**, 10457 (1994).
- <sup>10</sup> A. Nilsson, M. Weinelt, T. Wiell, P. Bennich, O. Karis, N. Wassdahl, J. Stöhr, and M. G. Samant, Phys. Rev. Lett. **78**, 2847 (1997); A. Nilsson, P. Bennich, T. Wiell, N. Wassdahl, N. Mårtensson, J. Nordgren, O. Björneholm, and J. Stöhr, Phys. Rev. B **51**, 10244 (1995).
- <sup>11</sup> H. Smolinski, C. Gros, W. Weber, U. Peuchert, G. Roth, M. Weiden, and C. Geibel, Phys. Rev. Lett. **80**, 5164 (1998).
- <sup>12</sup> M. Isobe and Y. Ueda, Phys. Soc. Jpn. **65**, 1178 (1996).
- <sup>13</sup> S.-H. Lee, Y. Qiu, C. Broholm, Y. Ueda, and J. J. Rush, Phys. Rev. Lett. **86**, 5554 (2001).
- <sup>14</sup> R. Valenti *et al.*, Phys. Rev. Lett. **86**, 5381 (2001).
- <sup>15</sup> Y. Harada *et al.* Phys. Rev. B **61**, 12 854 (2000).
- <sup>16</sup> G. T. Woods, G. P. Zhang, T. A. Callcott, L. Lin, G. S. Chang, B. Sales, D. Mandrus and J. He, (accepted to Phys. Rev. B, 2001); G. P. Zhang, T. A. Callcott, G. T. Woods, L. Lin, B. C. Sales, D. Mandrus, and J. He, Phys. Rev. Lett. **88**, 077401 (2002).
- <sup>17</sup> For a recent review, see W. E. Pickett, Comput. Phys. Rep. **9**, 115 (1989).
- <sup>18</sup> W. Kohn and L. J. Sham, Phys. Rev. **140**, 1133 (1965).
- <sup>19</sup> D. M. Ceperley and B. J. Alder, Phys. Rev. Lett. **45**, 566 (1980); J. P. Perdew and A. Zunger, Phys. Rev. B **23**, 5048 (1981).
- <sup>20</sup> E. L. Shirley, X. Zhu, and S. G. Louie, Phys. Rev. B **56**, 6648 (1997), and references therein.
- <sup>21</sup> E. L. Shirley, Phys. Rev. B **54**, 16464 (1996).
- <sup>22</sup> J. Garcia and M. Benfatto, Phys. Rev. Lett. **87**, 189701 (2001), J. E. Lorenzo, S. Bos, S. Grenier, H. Renevier, and S. Ravy, *ibid.*, 189702 (2001), and H. Nakao, K. Ohwada, N. Takesue, Y. Fujii, M. Isobe, Y. Ueda, M. v. Zimmermann, J. P. Hill, D. Gibbs, J. C. Woicik, I. Koyama, and Y. Murakami, *ibid.* 189703 (2001).

FIG. 1. (a)  $\text{NaV}_2\text{O}_5$  structure; (b) Experimental geometry.

FIG. 2. Experimental x-ray absorption spectra of  $\text{NaV}_2\text{O}_5$  at (a) the V  $L_3$  edge and (b) the O  $K$  edge. The angle  $\theta$  is between the electric polarization and the b axis.  $\theta$  increases from  $7.5^\circ$  to  $75^\circ$  in steps of  $7.5^\circ$ . The scan is in the b-c plane. The vertical dashed lines denote the positions of peaks A, B and C at 530.6, 532.1 and 532.8 eV, respectively.

FIG. 3. Intensities versus the polarization angle  $\theta$  for peaks A, B and C in Fig. 2(b).

FIG. 4. Theoretical absorption spectra of  $\text{NaV}_2\text{O}_5$  at the O  $K$  edge. (a) Total absorption spectra at the O  $K$  edge. Contributions are from (b)  $\text{O}_1$ , (c)  $\text{O}_2$  and (d)  $\text{O}_3$ . The scan condition is same as in Fig. 2. The arrows denote the change in intensity while varying polarization from along the b axis to along the c axis.

FIG. 5. Oxygen orbitals' spatial distributions in  $\text{NaV}_2\text{O}_5$ .

FIG. 6. Theoretical V  $L_3$  edge absorption. (a) Only the channels  $l = 1$  and  $m = 0$  is calculated; (b) Only the channel  $l = 1$  and  $m = \pm 1$  are calculated. (c) Total absorption spectrum at the V  $L_3$  edge. The scan condition is exactly same as in Fig. 2. The arrows have the same meaning as in Fig. 4.

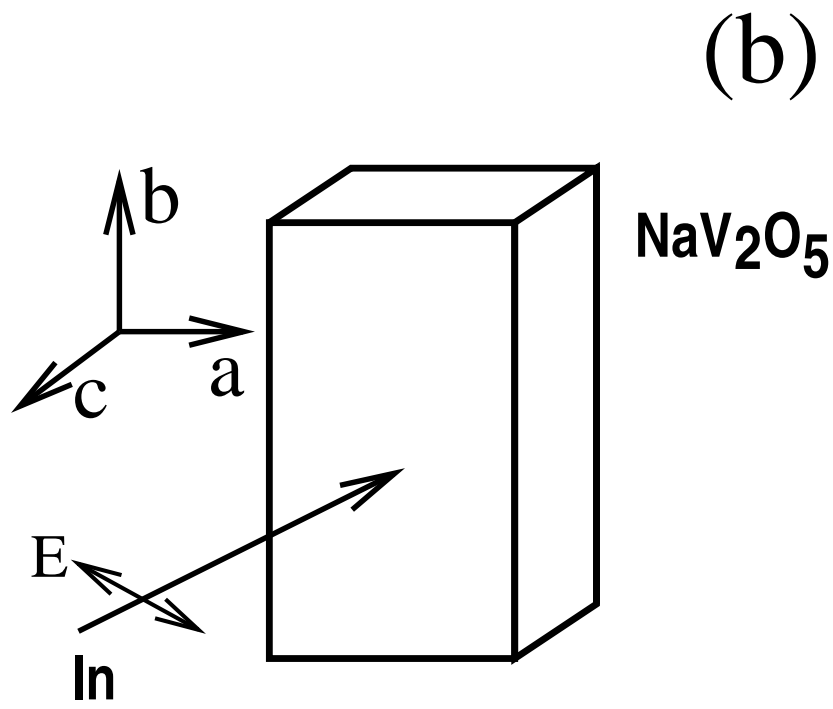
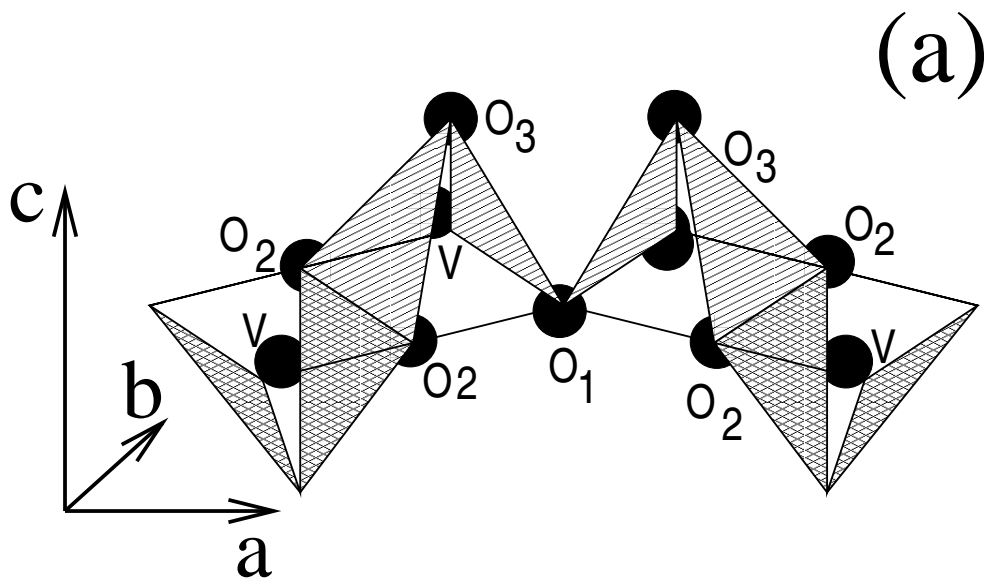


Figure 1

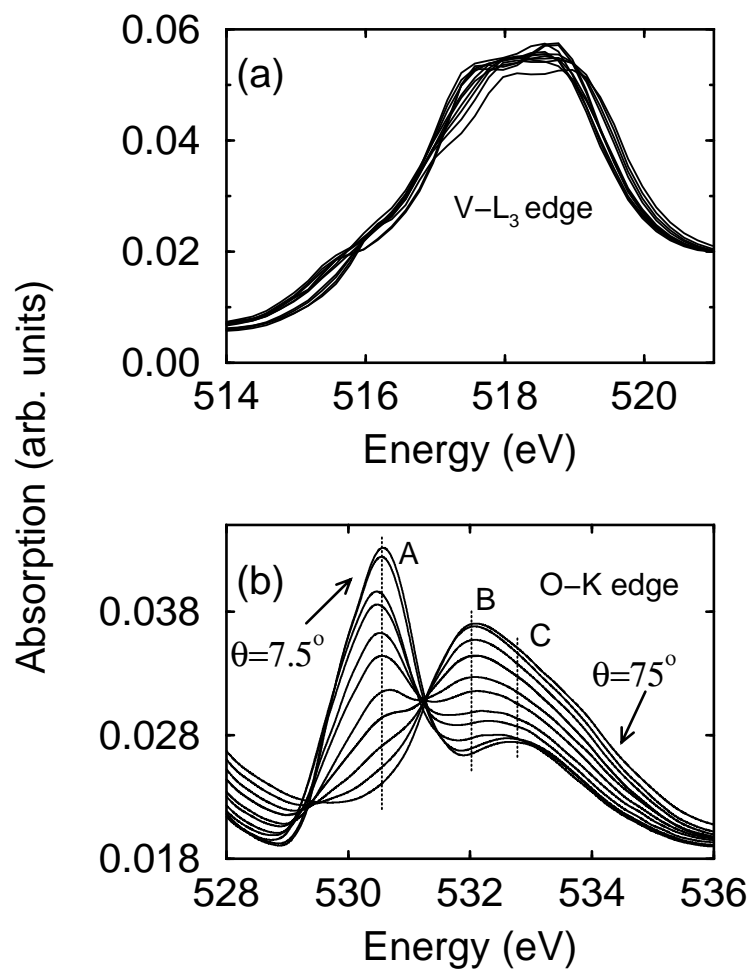


Figure 2



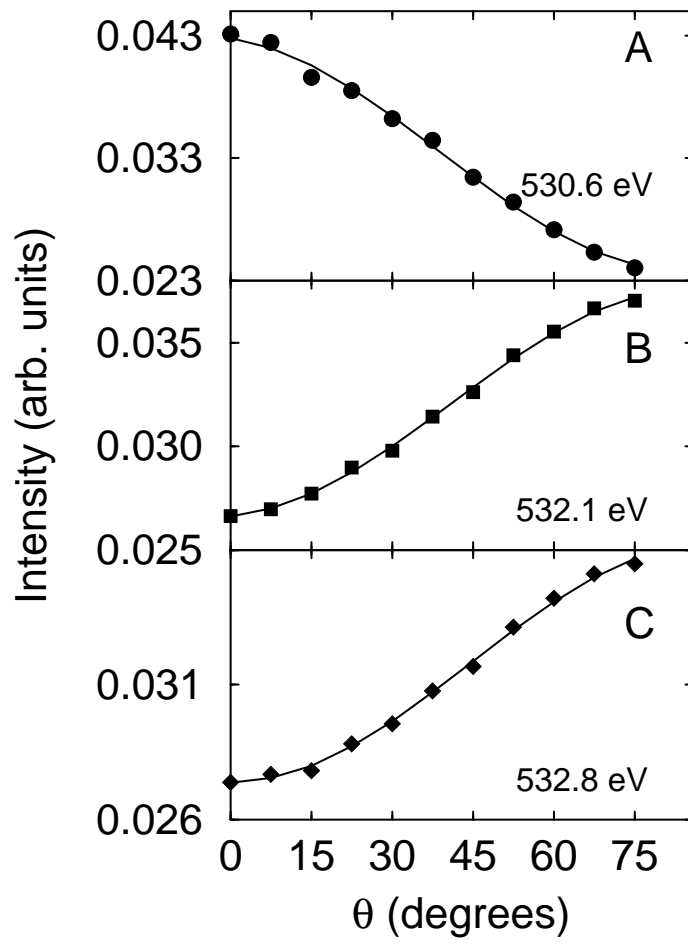


Figure 3

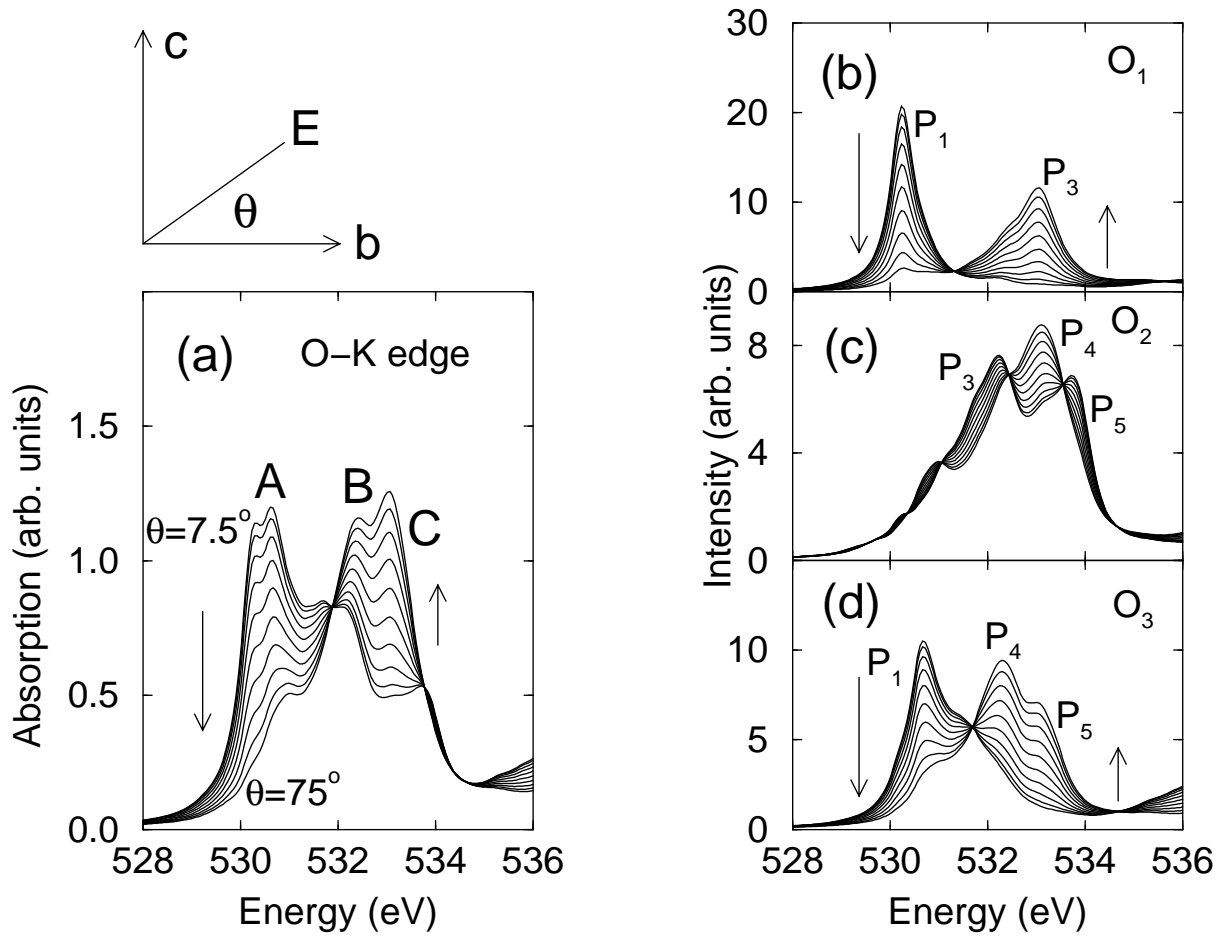


Figure 4

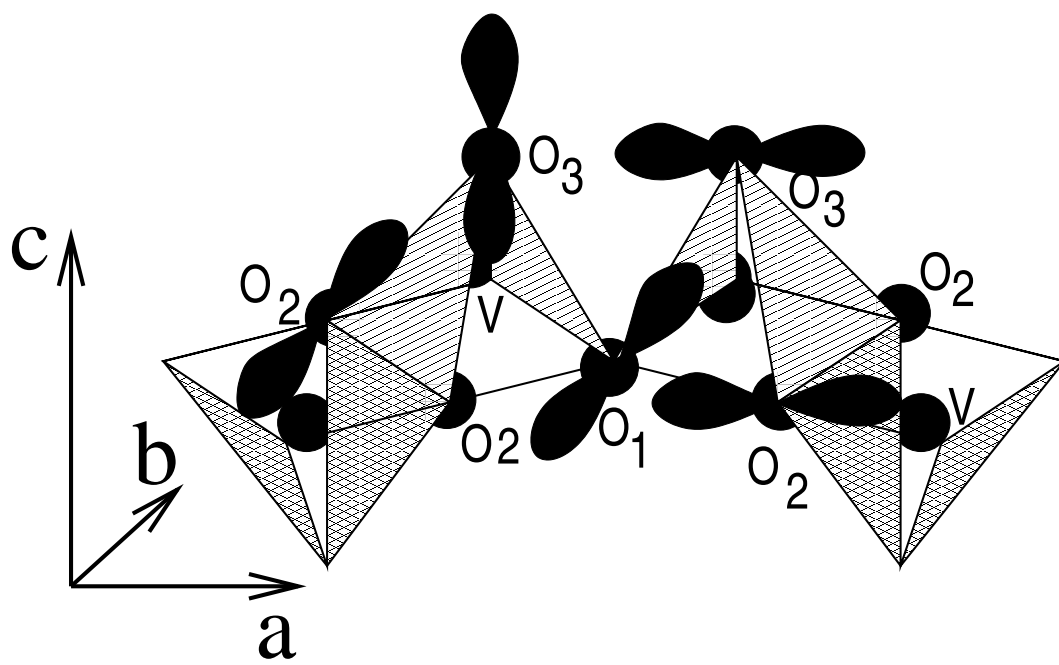


Figure 5

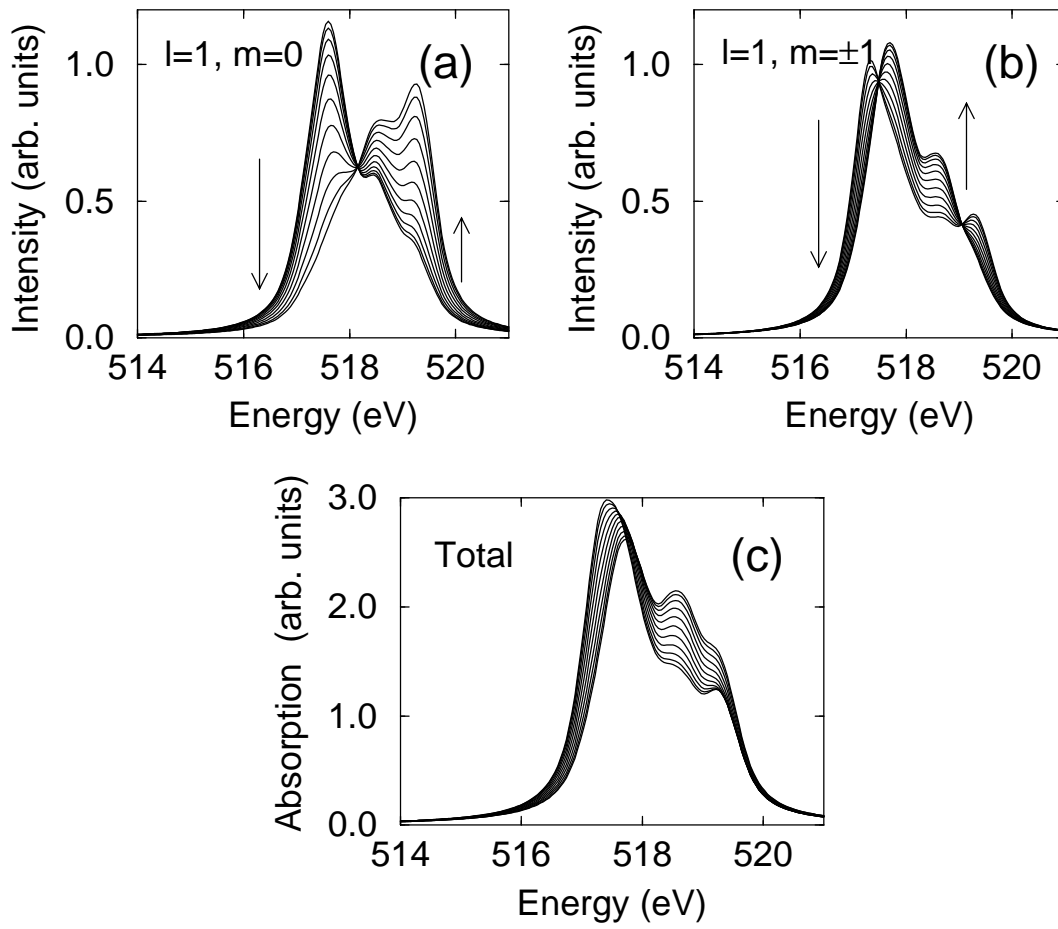


Figure 6